Original Article

# 18F-fluorodeoxyglucose positron emission tomography-computed tomography in the localization of the lesions in the osteogenic region of breast cancer bone metastases after therapy

**Runlong Lin[1#^], Huiyun Lv[2#], Jing Yu[1#^], Chen Song[2], Aijuan Tian[1^]**

[1]Department of Nuclear Medicine, The Second Hospital of Dalian Medical University, Dalian, China; [2]Department of Oncology, The Second Hospital of Dalian Medical University, Dalian, China

*Contributions:* (I) Conception and design: A Tian, C Song; (II) Administrative support: J Yu; (III) Provision of study materials or patients: H Lv, C Song; (IV) Collection and assembly of data: R Lin, A Tian; (V) Data analysis and interpretation: R Lin, A Tian; (VI) Manuscript writing: All authors; (VII) Final approval of manuscript: All authors.

[#]These authors contributed equally to this work.

*Correspondence to:* Aijuan Tian, MD. Department of Nuclear Medicine, The Second Hospital of Dalian Medical University, 467 Zhongshan Road, Shahekou District, Dalian 116023, China. Email: taj1870@163.com; Chen Song, MD. Department of Oncology, The Second Hospital of Dalian Medical University, 467 Zhongshan Road, Shahekou District, Dalian 116023, China. Email: 635320758@qq.com.

**Background:** Accurate efficacy evaluation of bone metastases (BMs) from breast cancer (BC) is an intractable issue in clinical practice, for which solutions are urgently needed. This study aimed to investigate the utility of 18F-fluorodeoxyglucose positron emission tomography-computed tomography (18F-FDG PET/CT) in the response evaluation of bone metastasis of BC.

**Methods:** In total, 22 patients diagnosed with BC and BM were enrolled. These patients underwent repeated 18F-FDG PET/CT evaluations. The patients and each BM site were divided into two groups based on their response to treatment: progressive disease (PD) and nonprogressive disease (non-PD). We analyzed and compared the changes in PET and CT images, as well as the serum concentration of carcinoembryonic antigen (CEA), carbohydrate antigen 153 (CA153), alkaline phosphatase (ALP), and calcium (Ca) over the same time frame. The immunohistochemistry (IHC) of primary lesions between groups and between the primary focus and BM with high 18F-FDG uptake were compared and analyzed.

**Results:** Maximum standard uptake value (SUVmax) after therapy [area under the curve (AUC): 0.932] and Δ-value of SUVmax (AUC: 0.811) on 18F-FDG PET imaging proved significantly valuable for the efficacy of therapy outcomes related to BM lesions ($P<0.05$). In terms of overall evaluation of BM, age and human epidermal growth factor receptor 2 (HER2) expression were significantly lower in the PD group than in the non-PD group ($P<0.05$). There were marked differences in CEA after therapy, the changes of CEA, and CA153 (Δ-value) between the groups ($P<0.05$). The SUVmax and Ca concentration after therapy and Δ-value of SUVmax, along with the levels of CA153, CEA, and ALP, were valuable indicators for evaluating the efficacy of individual BMs ($P<0.05$). IHC of BM in the PD group showed differences compared to primary lesions, with antigen Ki-67 being downregulated in metastatic lesions and HER2 being downregulated in a portion of BMs (2 of 6). Meanwhile, the expression of estrogen receptor (ER) and progesterone receptor (PR) remained relatively unchanged.

**Conclusions:** 18F-FDG PET/CT confers precise assessment of the posttreatment efficacy pertaining to BM in BC. This modality facilitates the identification of poor effect lesions following extant therapies and

^ ORCID: Runlong Lin, 0000-0002-6724-972X; Jing Yu, 0000-0002-3208-0821; Aijuan Tian, 0000-0002-7952-1807.

localization for pathological assessment and may substantially contribute to evaluating therapeutic efficacy, refining treatment strategies, and predicting the disease trajectory of patients with BC and BM.

**Keywords:** Breast carcinoma; bone metastases (BMs); positron emission tomography (PET); glucose metabolism imaging; efficacy assessment

Submitted Dec 06, 2023. Accepted for publication May 30, 2024. Published online Jun 26, 2024.
doi: 10.21037/qims-23-1738
**View this article at:** https://dx.doi.org/10.21037/qims-23-1738

## Introduction

Breast cancer (BC) stands as the predominant malignancy afflicting women globally, ranking second in cancer-related fatality across both the developed and developing world (1,2). Despite considerable advancements being made its management, BC remains an intractable disease, with certain patients progressing to advanced stages and often mortality fatality. Notably, distal metastases frequently manifest in sites, including the bones, lungs, liver, and brain. Of these, bone involvement is the most common, affecting over 70% of those with metastatic BC (3,4). This type of bone metastasis often leads to skeletal-related events, encompassing pathological fractures, pain, neural compression, and hypercalcemia. A panoply of targeted therapeutic approaches tailored to this context (e.g., bone-modifying agents) is currently available. The evaluation of posttherapeutic bone metastases (BMs) is critical to devising effective treatment plans. Although pathology is the gold standard for the diagnosis of bone metastasis, imaging plays an important role in the diagnosis and response monitoring of BMs in BC. The diagnosis and outcomes of BC BMs include osteogenic, osteogenic, and mixed changes. The osteogenic and mixed changes after treatment may include metastatic lesion progression or osteogenic repair after therapy. According to the Response Evaluation Criteria in Solid Tumors (RECIST) guideline (version 1.1), osteolytic or mixed lesions without soft tissue components and osteogenic lesions are considered as nonevaluable lesions (5). Computed tomography (CT) was hitherto employed to discern response through lesion resolution or sclerosis, but this approach has since been acknowledged to be insufficiently sensitive and requires at least half a year for a robust assessment of response (6-9). 18F-fluorodeoxyglucose-positron emission tomography integrated with computed tomography (18F-FDG PET/CT) can reflect the glucose metabolism, and change in 18F-FDG uptake before and after treatment of BMs (osteolytic, osteogenesis, mixed) can be sensitively detected; thus, it has been recognized as an objective and reliable indicator of bone metastasis response (10,11). BC is a highly heterogeneous tumor, and it is exceedingly common for primary and metastatic lesions to progress again after a period of stabilization or improvement. The lesions respond inconsistently to the current treatment (effective or ineffective). Therefore the means to identifying those lesions unresponsive to current treatment and the timely and accurate detection of progressive lesions are crucial to the prognosis of patients. Even with the help of traditional imaging modalities, such as CT, magnetic resonance imaging (MRI), and bone scintigraphy (BS), it remains difficult to evaluate the response of BMs, especially in osteogenic and mixed areas. This study aimed to investigate the application value of 18F-FDG PET/CT in the response evaluation of bone metastasis of BC through retrospective analysis. We present this article in accordance with the STROBE reporting checklist (available at https://qims.amegroups.com/article/view/10.21037/qims-23-1738/rc).

## Methods

### *Patients and pathology*

A retrospective analysis was conducted on a total of 22 patients with BC with bone metastasis who were treated between August 2019 and October 2023. These patients underwent multiple 18F-FDG PET/CT evaluations at the Department of Nuclear Medicine, The Second Hospital of Dalian Medical University. All participants received a definitive diagnosis of infiltrating ductal carcinoma through pathological confirmation. The cohort underwent complete clinical profiles and were subjected to standardized follow-up extending beyond 6 months after the last PET/CT assessment. Participants lacking comprehensive clinical diagnosis and follow-up data, along with those experiencing inadequate follow-up duration, were excluded. For cases

 

where biopsy proved challenging or multiple bone lesions were evident, clinical diagnosis was considered sufficient. Confirmation through diagnosis was secured through alternative imaging modalities, including CT and MRI, and augmented by clinical follow-up. The average age of the patients at the initial PET/CT evaluation in this cohort was 48.9±11.8 years, and the age range was 34 to 67 years. Among the 22 patients, the initial stage distribution was as follows: 1 patient at stage 0, 4 patients at stage I, 3 patients at stage II, 8 patients at stage III, and 6 patients at stage IV. On average, each patient underwent 2.41±0.73 PET/CT evaluations, with the number of evaluations ranging from 2 to 4. The average time interval between consecutive PET/CT evaluations was 13.4±8.5 months, with a range of 2 to 40 months. This study was conducted in accordance with the Declaration of Helsinki (as revised in 2013) and was approved by the Ethics Committee of The Second Hospital of Dalian Medical University (2022-103). The requirement for individual consent in this retrospective analysis was waived.

### *Imaging protocol*

A fasting duration of at least 6 hours preceded the intravenous injection. Administered activity was dosed proportionally to the patient's body weight (ranging between 3.70 and 5.55 MBq/kg). PET images, captured 60 minutes after intravenous injection, spanned from the cranial region to the mid-thigh and were captured with a PET/CT scanner (Ingenuity TF, Philips, Amsterdam, the Netherlands). The images underwent assessment with both scatter-corrected (SC) and attenuation-corrected (AC) PET modalities. For localization and attenuation correction, a CT scan ensued, consisting of 120 kV with automatic milliamperage selection (ranging between 25 and 150 mA). In immediate sequence to the CT scan, PET data were recorded over 3 minutes per bed. Reconstruction of the data set was completed with a slice thickness of 4 mm. The reconstruction adhered to the clinical standard, leveraging the proprietary blob-basis function ordered-subsets time-of-flight (BLOB-OS-TF) algorithm furnished by the PET/CT scanner manufacturer (Philips), incorporating reconstructed time-of-flight data.

Routine follow-up consisted of chest, abdomen, and pelvis CT scans. Manipulation of window width (WW) and window level (WL) was used to calibrate the CT image to accommodate bone alterations [WW: 1,000–1,500 Hounsfield units (HU); WL: 250–350 HU]. The CT imaging maintained a 4-mm slice thickness.

### *Clinical data collection*

Comprehensive compilation encompassed the initial stage, molecular subtypes, pathology, and the immunohistochemistry (IHC) of primary breast lesions and BMs. The parameters included estrogen receptor (ER), progesterone receptor (PR), human epidermal growth factor receptor 2 (HER2), and Ki-67 expression. Furthermore, we measured the serum tumor biomarkers associated with BC [carcinoembryonic antigen (CEA) and carbohydrate antigen 153 (CA153)], serum alkaline phosphatase (ALP), and serum calcium (Ca) ion concentration derived from patients undergoing 18F-FDG PET/CT and CT during the corresponding time frames.

### *Image analysis and efficacy assessment*

Two groups of clinicians, each comprising a nuclear medicine physician and an oncologist, undertook the evaluation of BMs. These medical professionals independently assessed metastatic status based on changes discerned in PET/CT, CT scans, and clinical data. Remarkable interrater concordance was observed between the two groups of clinicians. For any discrepancies, agreement was reached through exhaustive deliberation. In the evaluation of the skeletal lesions response, we considered the clinical symptoms, changes in serological indicators, changes in lesions glucose metabolism, and bone density. The European Organization for Research and Treatment of Cancer (EORTC) criteria can be used to identify heterogeneous responses after treatment. Since this study mainly focused on the heterogeneity of BMs and examined lesions that did not respond to therapy, the EORTC criteria were used for PET assessment (10). Response in bone density change after therapy was defined according to the classical World Health Organization (WHO) and Union for International Cancer Control (UICC) criteria (7,8). The patients were divided into progressive disease (PD) and nonprogressive disease (non-PD) groups. The non-PD group included the improvement and stable cases. The criteria for the improvement group were as follows: (I) pain mitigation at the lesion; (II) diminished serum concentrations of tumor biomarkers, ALP, and Ca; (III) CT scans revealing decreased extent of osteolytic lesions or osteogenesis; and (IV) a reduction greater than 25% in the tumor maximum standard uptake value (SUVmax) in lesions

 

observed on the baseline PET scan.

The PD group was defined according to the following criteria: (I) exacerbated pain at the lesion; (II) escalation in serum concentrations of tumor biomarkers, ALP, and Ca; (III) CT scans evidencing lesion enlargement or emergence of new osteolytic foci; (IV) and an increase in 18F-FDG tumor SUV of greater than 25% within the tumor region defined on the baseline scan, visible increase in the extent of 18F-FDG tumor uptake (20% in the longest dimension), or the appearance of new 18F-FDG uptake in metastatic lesions. Lesions not precisely aligning with the aforementioned criteria were classified as stable. The bone lesions in every group were required to meet at least one of the clinical manifestations (changes in clinical symptoms or serum blood indicators), must accorded with at least one of the imaging changes. When there was a conflict between the efficacy evaluation results of PET and CT, the PET result as a conclusive indicator.

Meticulous recording of the SUVmax via 18F-FDG PET imaging served to reflect the detailed profile of BMs. The density of lesions indicated by CT imaging was also scrupulously documented. We took into account both changes in bone density degree and distribution. There are four forms of bone density changes in the diagnosis and treatment of BMs: osteolytic, normal, mixed and osteoblastic. Mixed foci, were divided into patchy high-density foci with indistinct margins and ground-glass high-density foci. To facilitate statistical analysis, the specific distribution of bone density was graded according to degree as follows: 4 for well-demarcated nodular high-density foci, 3 for high-density foci with blurred margins, 2 for ground-glass high-density foci, 1 for normal density, and 0 for low-density foci.

### *Statistical analysis*

Statistical analysis was performed using SPSS version 22.0. The normality of continuous variables was assessed using the Shapiro-Wilk test. Normally distributed data are presented as the mean ± standard deviation ($\bar{x}$ ± s), while nonnormally distributed data are presented as median and interquartile range (IQR). Analysis of variance was used to compare normally distributed continuous variables between multiple groups. The chi-square test was used for frequency comparison between multiple groups. Independent samples *t*-tests were used to compare normally distributed continuous variables between two groups, while the Mann-Whitney test was used for to compare nonnormally distributed continuous variables between two groups. The diagnostic efficacy of various indicators in evaluating efficacy was assessed using receiver operating characteristic (ROC) curve analysis. P<0.05 was considered to indicate statistical significance.

## Results

No obvious correlation was found between the initial stage, subtype, and response of BMs, the expression of HER2 in the primary lesion of the PD group was lower than that of the non-PD group.

Efficacy evaluation proceeded on a patient-centric basis, involving a cohort of 22 patients who underwent 53 PET/CT examinations in total. A cumulative total of 31 efficacy assessments were conducted during proximate PET/CT evaluations. According to the criteria for response of BMs described above, 19 cases were defined as non-PD and 12 as PD. There was no obvious correlation between the initial stage, the subtype, or the response of BMs (initial stage: $X^2$=4.165, P=0.526; subtype: $X^2$=9.961, P=0.076). The proportion of patients with HER2 low expression in the primary lesion of PD group was significantly higher than that in the non-PD group ($X^2$=4.010; P=0.045) (see *Table 1*).

Younger age and lower HER2 expression within primary breast carcinoma lesions was associated with prognosis, and higher serum CEA levels after therapy and increased serum CEA the and CA153 concentration could aid in detecting the progression of BMs.

In terms of the overall patient efficacy evaluation, the age of the PD group was younger than that of the non-PD group (P<0.05), the CEA concentration after therapy and the Δ-value of CEA and CA153 in PD group were significantly higher than those in the non-PD group (P<0.05). Analysis of the basic clinical data indicated that only HER2 expression within the primary breast lesion was significantly different between the two groups (P<0.05). Lower HER2 expression correlated with an increased likelihood of suboptimal disease control (*Table 2*).

In terms of the sequential follow-up evaluations, the glucose metabolic intensity of PET (SUVmax) after therapy, the change of SUVmax, serum tumor biomarker level, (CEA, CA153), and ALP concentration could be used for efficacy assessment; meanwhile, the density and changes of BMs demonstrated middling performance for efficacy evaluation.

For the efficacy assessment of individual BMs, a total of 130 BMs were subjected to assessment via 18F-FDG PET/

 

**Table 1** Patient information and the response of bone metastases

| Patient | Initial clinical stage | TNM stage | Molecular typing of breast lesions | Frequency of PET examinations | Comparison frequency of PET | Response of bone metastases | Number of bone metastases included in the study | Comparison of frequency of bone lesions |
|---|---|---|---|---|---|---|---|---|
| 1 | IV | T1N2M1 | HER2 enriched | 2 | 1st | Non-PD | 3 | 3 |
| 2 | III | T1N3M0 | Luminal B (HER2 negative) | 3 | 1st | PD | 5 | 10 |
| | | | | | 2nd | PD | | |
| 3 | III | T3N1M0 | Luminal B (HER2 positive) | 2 | 1st | Non-PD | 1 | 1 |
| 4 | II | T2N1M0 | HER2 enriched | 2 | 1st | Non-PD | 3 | 1 |
| 5 | III | T1N2M0 | Triple negative | 4 | 1st | Non-PD | 5 | 15 |
| | | | | | 2nd | Non-PD | | |
| | | | | | 3rd | PD | | |
| 6 | IV | T2N1M1 | HER2 enriched | 4 | 1st | Non-PD | 5 | 15 |
| | | | | | 2nd | Non-PD | | |
| | | | | | 3rd | PD | | |
| 7 | IV | T2N1M1 | Luminal B (HER2 negative) | 2 | 1st | PD | 5 | 5 |
| 8 | 0 | TisN0M0 | Luminal A | 2 | 1st | Non-PD | 1 | 1 |
| 9 | II | T2N1M0 | Luminal B (HER2 negative) | 3 | 1st | Non-PD | 1 | 2 |
| | | | | | 2nd | Non-PD | | |
| 10 | III | T4N0M0 | Luminal B (HER2 negative) | 2 | 1st | PD | 5 | 5 |
| 11 | I | T1N0M0 | Luminal B (HER2 negative) | 2 | 1st | PD | 9 | 9 |
| 12 | III | T1N3M0 | Luminal B (HER2 negative) | 4 | 1st | Non-PD | 6 | 18 |
| | | | | | 2nd | PD | | |
| | | | | | 3rd | PD | | |
| 13 | I | T1N0M0 | Triple negative | 2 | 1st | PD | 5 | 5 |
| 14 | IV | T2N3M1 | Luminal A | 2 | 1st | Non-PD | 5 | 5 |
| 15 | I | T1N1M0 | Luminal B (HER2 positive) | 3 | 1st | PD | 5 | 10 |
| | | | | | 2nd | Non-PD | | |
| 16 | II | T2N0M0 | Triple negative | 2 | 1st | PD | 5 | 5 |
| 17 | III | T4N3M0 | HER2 enriched | 2 | 1st | Non-PD | 5 | 5 |
| 18 | III | T1N2M0 | Luminal B (HER2 negative) | 2 | 1st | Non-PD | 5 | 5 |
| 19 | III | T3N1M0 | Luminal B (HER2 positive) | 2 | 1st | Non-PD | 1 | 1 |
| 20 | IV | T1N2M0 | HER2 enriched | 2 | 1st | Non-PD | 3 | 3 |
| 21 | I | T1N1M0 | Luminal A | 2 | 1st | Non-PD | 5 | 5 |
| 22 | IV | T2N1M1 | HER2 enriched | 2 | 1st | Non-PD | 1 | 1 |
| Total | | | | 53 | 31 | Non-PD 19; PD 12 | 89 | 130 |

TNM, tumor-node-metastasis; PET, positron emission tomography; non-PD, non-progressive disease; PD, progressive disease; HER2, human epidermal growth factor receptor 2.

**Table 2** Comparative analysis of clinical indicators between the two efficacy groups (n=31)

| Characteristic | Non-PD (n=19) | PD (n=12) | P |
|---|---|---|---|
| Age, ($\bar{x}$ ± s), (years) | 52.47±12.70 | 42.67±7.23 | 0.010* |
| CEA, M (P25, P75), (ng/mL) | | | |
| Before | 1.16 (0.56, 2.20) | 1.75 (0.50, 27.34) | 0.671 |
| After | 0.62 (0.59, 1.41) | 5.37 (0.62, 131.59) | 0.021* |
| Δ-value | −0.12 (−0.41, 0.00) | 0.70 (0.00, 31.42) | 0.030* |
| CA153, M (P25, P75), (U/mL) | | | |
| Before | 9.30 (6.07,16.66) | 8.55 (5.24, 26.09) | 0.744 |
| After | 6.19 (4.92, 11.25) | 11.27 (4.68, 64.58) | 0.325 |
| Δ-value | −1.78 (−3.84, 1.44) | 3.15 (−1.98, 54.05) | 0.043* |
| ALP, M (P25, P75), (U/L) | | | |
| Before | 96.45 (52.51, 130.55) | 68.78 (57.89, 95.50) | 0.370 |
| After | 79.77 (61.26, 105.36) | 100.77 (56.18, 135.48) | 0.813 |
| Δ-value | 4.52 (−49.97, 31.66) | 8.67 (−5.41, 52.09) | 0.211 |
| Ca, M (P25, P75), (mmol/L) | | | |
| Before | 2.40 (2.26, 2.45) | 2.42 (2.33, 2.44) | 0.679 |
| After | 2.42 (2.34, 2.47) | 2.38 (2.28, 2.49) | 0.525 |
| Δ-value | 0.06 (−0.02, 0.06) | −0.05 (−0.17, 009) | 0.152 |
| ER ($\bar{x}$ ± s) | 1.09±1.1.20 | 1.33±0.0.98 | 0.520 |
| PR ($\bar{x}$ ± s) | 0.84±1.07 | 0.75±0.0.62 | 0.833 |
| HER2 ($\bar{x}$ ± s) | 2.24±1.42 | 1.42±0.90 | 0.013* |
| Ki-67 ($\bar{x}$ ± s) | 39.12±25.69 | 47.91±27.09 | 0.382 |

*, P<0.05. Non-PD, non-progressive disease; PD, progressive disease; $\bar{x}$, mean; s, standard deviation; CEA, carcinoembryonic antigen; M, median; P25, 25th percentile; P75, 75th percentile; CA153, carbohydrate antigen 153; ALP, alkaline phosphatase; Ca, calcium; Before, pretreatment serum concentration; After, posttreatment serum concentration; Δ-value, change in serum concentration before and after treatment; ER, estrogen receptor expression of breast primary lesion; PR, progesterone receptor expression of breast primary lesion; HER2, human epidermal growth factor receptor 2 of the breast primary lesion; Ki-67, antigen Ki-67 expression of the breast primary lesion.

CT and conventional CT, both before and after therapy. The status of BMs at baseline (prior to treatment) was compared to that after change in treatment plan. After treatment, 93 lesions were assessed as non-PD, while 37 lesions were assessed as PD. Notably, SUVmax values derived from 18F-FDG PET were significantly higher at baseline in the PD group than in the non-PD group, and the SUVmax level in the PD group significantly increased compared to baseline (P<0.05). There was an increase in bone density at lesion sites compared to baseline, and significant differences were noted between the baseline and the two groups (P<0.05). However, there was no difference in bone density change between the two groups posttreatment (P>0.05) (*Table 3*).

A comprehensive comparison was conducted between the non-PD and PD groups, with all indicators being considered. Remarkably, the SUVmax after therapy and the change in SUVmax, CEA, CA153, and ALP levels before and after therapy showed diagnostic value in distinguishing therapeutic efficacy (P<0.05). Although there was a significant difference in bone density observed on CT scans before therapy between the two groups (P<0.05), there was no significant difference in bone density after therapy or in the change of bone density before and after therapy (P>0.05). The posttreatment Ca levels in the PD group were lower than those in the non-PD group. In contrast, the indicators

 

**Table 3** Overview of 18F-FDG uptake and bone density before and after treatment of every bone metastasis (n=130)

| Characteristic | Baseline (n=130) | Non-PD (n=93) | PD (n=37) | P |
|---|---|---|---|---|
| PET ($\bar{x}$ ± s) | | | | |
| SUVmax | 4.78±3.49 | 1.22±0.13 | 6.44±2.53 | <0.001[*abcd] |
| CT (n) | | | | |
| Nodular high-density-4 | 18 | 21 | 5 | <0.001[*abc]; 0.446[d] |
| Patchy high-density-3 | 19 | 30 | 12 | |
| Ground-glass high-density-2 | 24 | 24 | 10 | |
| No abnormality-1 | 35 | 10 | 8 | |
| Low density-0 | 34 | 8 | 2 | |

*, P<0.05. [a], comparison between three groups (baseline, non-PD, and PD); [b], comparison between baseline and non-PD group; [c], comparison between baseline and PD group; [d], comparison between non-PD and PD group. 18F-FDG, 18F-fluorodeoxyglucose; non-PD, non-progressive disease; PD, progressive disease; PET, positron emission tomography; $\bar{x}$, mean; s, standard deviation; SUVmax, maximum standardized uptake value; CT, computed tomography.

that were not effective in determining therapeutic efficacy were CAE, CA153, and ALP levels before and after therapy; Ca levels before therapy; and the change in Ca levels after therapy (See *Table 4*).

The relevant indicators of PET demonstrated the highest ability to ascertain efficacy; changes in some serological indicators were significant in predicting the prognosis of the disease, while changes in CT density performed relatively poor in discriminating efficacy.

The ROC curve was plotted, and the efficacy assessment parameters underwent screening based on the comparison of the area under the curves (AUCs) for each index. The posttherapy SUVmax and the Δ-value of SUVmax emerged as the most precise metrics for efficacy evaluation, yielding AUCs of 0.932 and 0.811, respectively. Certain serological indicators provided certain value in efficacy assessment: the Δ-value of CA153 and the Δ-value of CEA yielded AUCs of 0.747 and 0.704, respectively, while the Δ-value of ALP yielded an AUC of 0.675. Blood Ca levels after treatment could also serve as a reference for evaluating the therapeutic effectiveness of BMs (AUC: 0.386), while lower blood Ca concentration indicated poor efficacy. The P values of these indices were all below 0.05, indicating a significant difference between the groups. Meanwhile, the other parameters, including CT-derived density changes, did not demonstrate significant intergroup differences (P>0.05) (See *Figure 1*, *Table 5*).

Compared with the pathological IHC of the primary lesion, the BMs in the PD group showed downregulation of Ki-67 and HER2 in some lesions.

Pathological analysis was performed on BMs in 6 of the 22 patients. The analysis focused on the bones that exhibited abnormal glucose metabolism as shown by PET imaging. The IHC phenotypes of the BMs were found to differ from those of the primary lesions, indicating the inherent heterogeneity in the process of tumor metastasis. It is worth noting that in these limited six cases, the expression of Ki-67 was downregulated to varying degrees. In one patient (Case 2), there was a difference in the subtype of the primary lesions (triple negative and luminal B). Although the molecular subtypes of the primary lesion and BMs were generally similar, there were two cases where the HER2 expression in the metastatic lesion was downregulated compared to that in the primary lesion (see *Figure 2*, *Table 6*).

## Discussion

With the steady advancement of medical science, a greater number of patients with advanced-stage tumors are able to receive successful treatment, leading to prolonged survival. However, owing to the inherent heterogeneity of tumors, certain primary and metastatic lesions recur despite effective intervention. The accurate identification of these lesions at an early stage and the precise assessment of their efficacy are pivotal to patient prognosis. Unlike the evaluation of other malignancies, alterations within treated BMs exhibit a range of complexities. Abnormal bone density increase can signify osteogenic repair, a limited presence of active tumor cells within an osteogenic repair background, or emerging osteogenic metastases. These interacting,

 

**Table 4** Intergroup and pairwise comparison of indicators between the two groups

| Characteristic | Non-PD (n=93) | PD (n=37) | P |
|---|---|---|---|
| PET (SUVmax) ($\bar{x}$ ± s) | | | |
| Before | 4.63±3.49 | 5.13±3.19 | 0.458 |
| After | 2.17±1.21 | 6.43±2.53 | <0.001* |
| Δ-value | –2.46±3.37 | 1.31±3.42 | <0.001* |
| CT ($\bar{x}$ ± s) | | | |
| Before | 1.70±1.44 | 1.46±1.19 | 0.003* |
| After | 2.49±1.20 | 2.27±1.12 | 0.446 |
| Δ-value | 0.80±1.24 | 0.81±1.37 | 0.978 |
| CEA (ng/mL), M (P25, P75) | | | |
| Before | 1.61 (0.50, 16.85) | 5.451.06, 31.62) | 0.054 |
| After | 1.16 (0.50, 32.81) | 1.47 (0.53, 94.47) | 0.471 |
| Δ-value | 0.00 (–0.50, 0.14) | 2.77 (0.00, 32.28) | <0.001* |
| CA153 (U/mL), M (P25, P75) | | | |
| Before | 9.30 (6.06, 28.08) | 9.10 (5.16, 102.00) | 0.937 |
| After | 6.68 (6.19, 11.74) | 5.60 (2.71, 25.85) | 0.167 |
| Δ-value | –0.39 (–3.31, 2.79) | 3.51 (2.09, 68.10) | <0.001* |
| ALP (U/L), M (P25, P75) | | | |
| Before | 91.00 (69.38, 130.90) | 85.93 (65.00, 123.25) | 0.787 |
| After | 71.11 (53.10, 137.00) | 66.00 (59.00, 97.00) | 0.392 |
| Δ-value | 4.52 (–43.60, 27.23) | 11.06 (–1.00, 56.60) | 0.002* |
| Ca (mmol/L), M (P25, P75) | | | |
| Before | 2.41 (2.31, 2.48) | 2.41 (2.32, 2.45) | 0.350 |
| After | 2.39 (2.31, 2.48) | 2.21 (2.15, 2.42) | 0.045* |
| Δ-value | 0.02 (–0.05, 0.09) | –0.05 (–0.20, 0.17) | 0.437 |

*, P<0.05. Non-PD, non-progressive disease; PD, progressive disease; PET, positron emission tomography; SUVmax, maximum standardized uptake value; $\bar{x}$, mean; s, standard deviation; Before, pretreatment serum concentration; $\bar{x}$, mean; s, standard deviation; After, posttreatment serum concentration; Δ-value, change in serum concentration before and after treatment; CT, computed tomography; CEA, carcinoembryonic antigen; M, median; P25, 25th percentile; P75, 75th percentile; CA153, carbohydrate antigen 153; ALP, alkaline phosphatase; Ca, calcium.

complex changes pose significant challenges to conventional imaging diagnostics. 18F-FDG PET, which targets regions manifesting abnormal glucose metabolism and identifies areas with active tumor cells, allows for the assessment of tumor status via the glucose metabolism, facilitating the determination of lesion status prior to anatomical transformations. This is critically important for patient treatment and prognosis.

Patients with BC are particularly susceptible to BMs, with the related changes after treatment being diverse. Precisely gauging the effectiveness of interventions on BMs constitutes a challenge in clinical practice. Prior nuclear medicine studies on diagnosing BMs in BC have predominantly focused on assessing the diagnostic sensitivity, specificity, and accuracy of 18F-FDG PET/CT (12). Our study examined the potential of 18F-FDG PET/CT in the posttreatment evaluation of BMs, with a specific emphasis on distinguishing between osteogenic

 

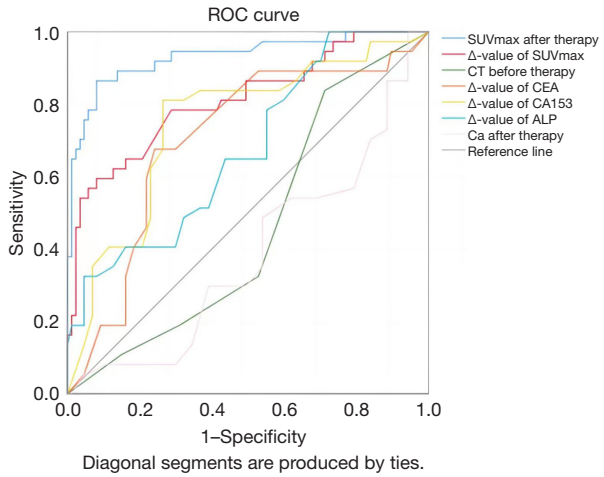


**Figure 1** ROC curves for indicators relevant to efficacy assessment. ROC, receiver operating characteristic; SUVmax, maximum standardized uptake value; After, posttreatment serum concentration; Δ-value, change in serum concentration before and after treatment; CT, computed tomography; Before, pretreatment serum concentration; CEA, carcinoembryonic antigen; CA153, carbohydrate antigen 153; ALP, alkaline phosphatase; Ca, calcium.

repair and active tumor tissue in the osteogenic region after the administration of antitumor therapy. Our findings suggest that regions displaying abnormal bone density grow, as observed through 18F-FDG PET scans with normal or absent 18F-FDG uptake, and this may signify osteogenic repair following treatment of metastatic lesions and not the presence of active tumors. Conversely, heightened 18F-FDG uptake implies the presence of active tumor cells and not therapeutically effective osteogenic repair.

Bone marrow stromal cells elicit the migration of tumor cells by expressing chemotactic molecules, thus providing a conducive growth milieu for tumor cells (13). The capacity of tumor cells to adhere to the bone matrix, fostering osteoclast maturation and activity, plays a pivotal role in the genesis of BMs. This primary osteoblastic activity might be indiscernible in imaging from the reactive and reparative osteoblastic activity that emerges after successful management of osteoblastic metastases (6). Depending on the chosen imaging modalities, the detection of metastatic bone tumor can be performed via two approaches: direct identification of the tumor and its tissue infiltration or

**Table 5** ROC curves for the various research indicators

| Variable | AUC (95% CI) | P |
|---|---|---|
| SUVmax after therapy | 0.932 (0.878–0.986) | <0.001* |
| Δ-value of SUVmax | 0.811 (0.723–0.900) | <0.001* |
| Δ-value of CA153 (U/mL) | 0.747 (0.651–0.844) | <0.001* |
| Δ-value of CEA (ng/mL) | 0.704 (0.602–0.806) | <0.001* |
| Δ-value of ALP (U/L) | 0.675 (0.574–0.776) | 0.002* |
| CEA before therapy (ng/mL) | 0.608 (0.492–0.720) | 0.057 |
| SUVmax before therapy | 0.564 (0.459–0.668) | 0.263 |
| CEA after therapy (U/mL) | 0.541 (0.432–0.649) | 0.476 |
| CA153 before therapy (U/mL) | 0.505 (0.377–0.632) | 0.937 |
| D-value of CT density | 0.489 (0.376–0.602) | 0.851 |
| ALP before therapy (U/L) | 0.485 (0.368–0.602) | 0.787 |
| CT density before therapy | 0.459 (0.354–0.564) | 0.471 |
| Δ-value of Ca (mmol/L) | 0.456 (0.325–0.587) | 0.438 |
| ALP after therapy (U/L) | 0.451 (0.346–0.557) | 0.393 |
| Ca before therapy (mmol/L) | 0.447 (0.333–0.561) | 0.352 |
| CT density after therapy | 0.427 (0.318–0.537) | 0.202 |
| CA153 after therapy (U/mL) | 0.422 (0.296–0.547) | 0.168 |
| Ca after therapy (mmol/L) | 0.386 (0.279–0.494) | 0.046* |

*, P<0.05. ROC, receiver operating characteristic; AUC, area under the curve; 95%CI, 95% confidence interval; SUVmax, maximum standardized uptake value; CT, computed tomography; CEA, carcinoembryonic antigen; CA153, carbohydrate antigen 153; ALP, alkaline phosphatase; Ca, calcium; Before, pretreatment serum concentration; After, posttreatment serum concentration; Δ-value, change in serum concentration before and after treatment.

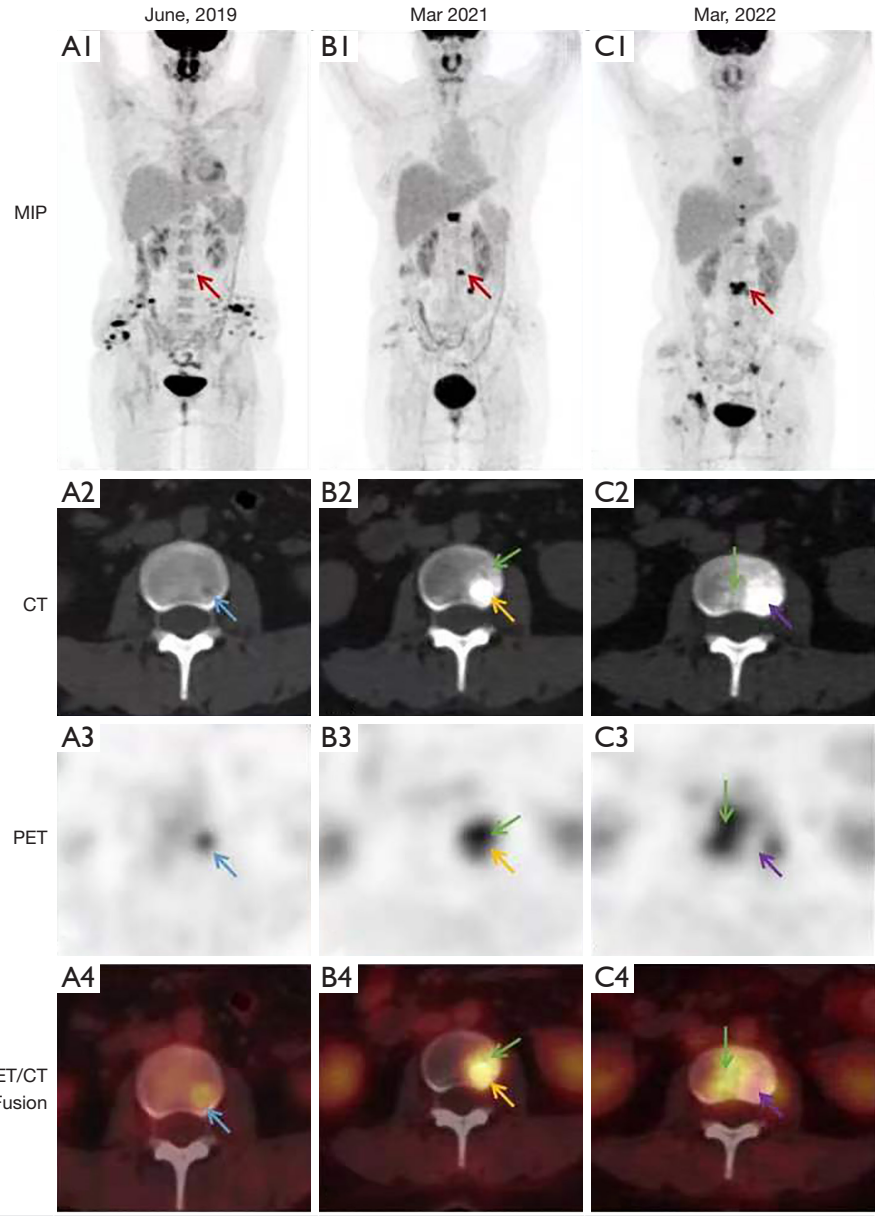


| | | | |
|---|---|---|---|
| CEA (ng/mL) | 1.61 | 30.43 | 159.02 |
| CA153 (U/mL) | 5.12 | 9.10 | 19.56 |
| Ca (mmol/L) | 2.41 | 2.43 | 2.50 |
| ALP (U/L) | 76.00 | 62.17 | 111.82 |

**Figure 2** A case of invasive ductal carcinoma of the left breast. A 38-year-old female patient. The primary lesion exhibited an immunohistochemical phenotype of ER (1+), PR (1+), and HER2 (1+). The initial PET/CT examination was conducted 2 years after surgery and systemic medical oncology therapy in June 2019. The patient's serological parameters (CEA, CA153, Ca, and ALP) were within the normal range. PET/CT revealed abnormal 18F-FDG uptake at the second lumbar vertebra (L2), with no other tumor-associated 18F-FDG uptake foci detected on the MIP image (A1). CT images displayed a low-density focus (6×8 mm) within the left half of the L2 (A2). PET and PET/CT fusion images (A3,A4) indicated significantly heightened 18F-FDG uptake (SUVmax 6.8) at the low-density focus and the perifocal bone with normal density. Subsequent pathological examination confirmed the presence of breast cancer metastasis, with ER–, PR–, and HER2 1+ status. PET/CT was conducted 18 months after the treatment regimen was administered (March 2021), with the

 

patient exhibiting elevated serum tumor markers (CEA and CA153) but stable Ca and ALP levels. The MIP image revealed an expanded and intensified range of radiotracer accumulation at the L2 and a new metastatic lesion at the 11th thoracic vertebra (T11) and the left psoas major muscle (L3 level) (B1). The previously observed low-density focus within the L2 had transformed into a high-density nodule (12×11 mm), with persistent high 18F-FDG uptake (SUVmax 6.8). Additionally, a ground-glass density region had emerged outside the nodule, displaying heightened 18F-FDG uptake (SUVmax 7.9). The patient was continued on the planned therapy, leading to another PET/CT examination year later due to escalating tumor markers, elevated Ca levels, and an increased ALP concentration (March 2022). Multiple BMs were discovered, along with fresh lesions in the right axilla and right lung. The range of radiotracer accumulation at the L2 was substantially expanded and included the involvement of the left psoas major muscle (C1). The nodular high-density focus exhibited an enlarged range (17×16 mm), and abnormal glucose metabolism was essentially absent (SUVmax 2.3). Notably, new regions of ground-glass density emerged around the area, displaying elevated glucose metabolism (SUVmax 9.2) (C2-C4). The red arrow indicates 18F-FDG uptake in the L2, the blue arrow indicates a low-density nodule with high 18F-FDG uptake, a yellow arrow indicates a high-density nodule with high 18F-FDG uptake, a green arrow indicates high 18F-FDG uptake in a ground-glass density region, and a purple arrow indicates a high-density nodule with low 18F-FDG uptake. MIP, maximum intensity projection; CT, computed tomography; PET, positron emission tomography; PET/CT fusion, positron emission tomography and computed tomography fusion imaging; CEA, carcinoembryonic antigen; CA153, carbohydrate antigen 153; Ca, calcium; ALP, alkaline phosphatase; ER, estrogen receptor; PR, progesterone receptor; HER2, human epidermal growth factor receptor 2; 18F-FDG, 18F-fluorodeoxyglucose; SUVmax, maximum standardized uptake value.

**Table 6** Comparison of pathological characteristics between primary lesions and bone metastases

| Patient | Focus | ER | PR | HER2 | Ki-67 (%) | Molecular typing |
|---|---|---|---|---|---|---|
| Case 1 | Primary | 1 | 1 | 1 | 80 | Luminal B (HER2 negative) |
| | BM | 1 | 0 | 1 | 30 | Luminal B (HER2 negative) |
| | BM | 0 | 0 | 1 | 10 | Triple negative |
| Case 2 | Primary | 0 | 0 | 0 | 70 | Triple negative |
| | Primary | 2 | 0 | 3 | 20 | Luminal B (HER2 positive) |
| | BM | 2 | 2 | 3 | 10 | Luminal B (HER2 positive) |
| Case 3 | Primary | 2 | 2 | 2 | 40 | Luminal B (HER2 negative) |
| | BM | 2 | 1 | 2 | 15 | Luminal B (no FISH testing, HER2 unknown) |
| Case 4 | Primary | 2 | 1 | 1 | 30 | Luminal B (HER2 negative) |
| | BM | 3 | 0 | 0 | 30 | Luminal B (HER2 negative) |
| Case 5 | Primary | 3 | 0 | 2 | 30 | Luminal B (HER2 positive) |
| | BM | 2 | 0 | 2 | 20 | Luminal B (HER2 positive) |
| Case 6 | Primary | 1 | 1 | 1 | 30 | Luminal B (HER2 negative) |
| | BM | 3 | 0 | 0 | 30 | Luminal B (HER2 negative) |

The categorization of ER, PR, and HER2 expressions relied on the findings of pathological examination and were classified as follows: negative assignment, 0; weak positive (1+), 1; moderate positive (2+), 2; and strong positive (3+), 3. Ki-67 expression was quantified as a positive percentage. ER, estrogen receptor; PR, progesterone receptor; HER2, human epidermal growth factor receptor 2; Ki-67, antigen Ki-67; BM, bone metastasis; FISH, fluorescence in situ hybridization.

the visualization of bone response in the presence of tumor cells. Osteoblastic metastasis is characterized by reduced bone resorption and an augmented stimulation of osteoblasts (14).

CT is a keystone imaging modality in the diagnosis of BMs, and it has long been a routine clinical methodology for assessing the efficacy the therapy for bone lesions, providing remarkable spatial resolution and the ability to evaluate bone trabeculae and cortical constituents (15). Nevertheless, CT lacks the capability to discriminate

 

between metabolically active and inert bone lesions, which impedes its ability to evaluate therapeutic efficacy. In this study, we stratified osteogenic lesions into five grades based on CT alterations. Subsequently, based on the observed alterations in the lesion state, we segregated BMs into two models: a sclerosis-improvement and stabilization model and a sclerosis-progression model. We found that when the CT value of BMs was increased, the precise condition of the lesion remained elusive.

MRI is also a staple clinical imaging diagnostic modality. It particularly excels in the diagnosis of bone marrow metastases, as it enables the early detection of lesions prior to the manifestation of its structural changes in bone and bone marrow. Nonetheless, MRI remains confined to local imaging and is insufficient for comprehensively diagnosing and appraising the entire body's bone and bone marrow condition. Furthermore, the intricate signal changes across various sequences within the lesion area posttreatment pose significant challenges to diagnostic imaging physicians. Thus, when other imaging assessments are unable to confirm the presence of a lesion at a specific site, local MRI examinations can prove valuable for diagnosis; however, its utility is confined to assessing the effectiveness of systemic bone and bone marrow lesions.

Radionuclide bone imaging, particularly whole-body static imaging (WBS), can offer insights into osteoblast activity and vascular networks within the skeleton. This technique exhibits a proclivity for tracer absorption at sites of vigorous bone formation (16,17). Although it is popular among clinicians, it is considered to be relatively insensitive and nonspecific for the assessment of systemic treatment response to BMs. Furthermore, radionuclide bone imaging often requires weeks or even months to confirm a treatment response (18-20). The flare phenomenon that follows chemotherapy or endocrine therapy can interfere with the differentiation between disease progression and reparative osteoblastic activity. Moreover, the temporal lag for accurately appraising treatment efficacy from the initiation of therapy ranges from 3 to 6 months, imposing constraints on the use of WBS for efficacy evaluation within routine clinical practice. Despite the advent and use of single-photon emission CT (SPECT) and CT, which provides anatomical localization and structural insights into skeletal lesions upon diagnosis, gauging the efficacy of radionuclide-concentrated osteogenic areas remains challenging. This study refrained from conducting a comparison between PET and SPECT due to the limited number of patients concurrently subjected to PET and SPECT. This will be addressed independently in future studies.

18F-FDG PET/CT serves as a precise method for appraising the treatment response of hypermetabolic bone and bone marrow metastases and is contingent upon the quantitative evaluation of 18F-FDG uptake. The metabolic effects engendered by treatment manifest earlier than do morphological changes. PET/CT has demonstrated superior sensitivity and specificity in comparison to conventional imaging modalities (21). PET/CT can directly identify the presence of tumor cells via the quantification of metabolic vigor, facilitating the detection of active tumor tissue throughout the body (22). Changes in SUVmax after treatment facilitate the differentiation between lesion improvement, stability, and progression, especially when guided by changes (Δ-value) before and after treatment. The uptake of 18F-FDG in viable BMs is primarily attributed to tumor cells of the primary BC and not bone cells, thus functioning as a tumor-specific tracer rather than as a direct reflection of the altered bone microenvironment (21). A decrease in 18F-FDG uptake during bone metastasis treatment may be attributed to osteoblast proliferation within BMs leading to augmented production of bone matrix and a concomitant relative decrease in cell density. This results in reduced 18F-FDG accumulation since tissue 18F-FDG uptake reflects the underlying glucose metabolism and cell density. The heightened sensitivity of PET compared to WBS may stem from its capacity to detect metastatic tumor cells prior to the full activation of osteoblasts within the bone marrow, thus facilitating the detection of bone-specific tracers (14,23).

A number of studies have demonstrated a strong correlation between alterations in 18F-FDG uptake and clinical and tumor-marker responses, suggesting that they may serve as predictive indicators until progression and skeletal-related events occur (24,25). In our study, the pre- and posttherapy serum tumor biomarkers (CEA and CA153), ALP concentration, and their change before and after therapy were indeed different between the groups and could support the evaluation of therapeutic efficacy. However, it is imperative to acknowledge that serum tumor markers reflect changes in tumor burden throughout the entire body, encompassing alterations within BMs. Thus, when a patient has metastases in other organs, the assessment of changes in bone lesions necessitates integration with changes in other tumor sites. Furthermore, the tumor markers fail to accurately locate the malignant lesions. In contrast, 18F-FDG PET excels at precisely and promptly identifying even a limited number of progressing lesions.

 

In our study, younger women had a higher probability of disease progression. Young age has been reported to be an independent risk factor of death or recurrence and is associated with a poor prognosis for BC. Although diagnostic delays may lead to a more advanced initial stage, biological differences nonetheless play an important role. It has been established that BC is more histologically aggressive in young women compared with their older counterparts (26).

BC is a highly heterogeneous tumor, and many lesions show therapeutic resistance during treatment due to changes in subtype or/and the expression of Ki-67. It is critical to implement the individualized treatment of BC on the basis of standardized treatment. 18F-FDG PET is highly suitable for finding the treatment-tolerant lesions (malignant foci) and guiding biopsy. 18F-FDG concentration in PET examination is associated with series of mechanisms including cell adhesion, invasion, metastasis, and antitumor gene downregulation. 18F-FDG uptake is also associated with the molecular subtypes of BC. Some researcher have asserted that HER2/ER-positive BC may be the most suitable BC subtype for 18F-FDG PET. HER2/ER-positive BC often has high Ki-67 levels, a marker of cell proliferative potential, and the PI3K/Akt/mTOR pathway is also activated. The phosphatidylinositol 3-kinase (PI3K)/Akt/mammalian target of rapamycin (mTOR) pathway is also involved in the expression and function of glucose transporters, which are involved in glucose uptake (27-29). Other studies have reported that 18F-FDG SUVmax is significantly associated with ER negativity, PR negativity, HER2 positivity, a high Ki-67 index, a larger tumor size, a higher histological grade, the presence of axillary lymph node metastasis, and a more advanced stage (30,31). Therefore, the uptake of 18F-FDG is associated to the subtype, with the triple-negative subtype and HER2-positive subtype showing a higher SUVmax and the luminal A subtype showing a lower SUVmax (32). In the six cases that we observed, compared with that of primary site, the Ki-67 of the metastatic sites were all downregulated to varying degrees; moreover, the molecular subtypes of the primary and metastatic lesions were basically the same, and only a portion of the BMs in PD group showed downregulation of HER2 (2/6), which is not consistent with the previous reports. Thus this may be attributed to our limited sample size and the lack of accounting for other factors that may contribute to suboptimal efficacy, which should be further explored by researchers and physicians.

Notably, our study revealed there to be a connection between the low expression of HER2 in primary breast carcinoma lesions and prognosis. Lower HER2 expression was correlated with an increased likelihood of suboptimal disease control. Pathological examination was carried out on regions demonstrating anomalous glucose metabolism as identified by 18F-FDG PET. This method can enable clinicians to promptly and accurately detect changes, allowing for timely treatment plan adjustments and ultimately enhancing patient prognosis.

There were certain limitations to this study which should be addressed. First, we employed a retrospective design and a limited sample size, particularly for the subgroups, which precluded the implementation of multivariate analysis. An additional constraint was the absence of quantitative assessments for bone metastasis state and HU due to the complexity of bone density changes after treatment of BMs; we will further attempt to address this challenge through image texture analysis.

## Conclusions

Alterations in bone density posttreatment can be observed via CT, and variations in serum tumor biomarkers for BC (CEA, CA153), serum ALP, and serum Ca may be valuable for the assessment of therapeutic outcomes in BC BMs; however, their discriminatory capacity diminishes in conditions involving multiple posttreatment changes. In contrast, the fluctuations in bone glucose metabolism depicted by 18F-FDG PET provide an effective means of discerning the posttreatment conditions in BMs, offering accurate identification of lesions resistant to prevailing treatments. Consequently, 18F-FDG PET/CT may be highly valuable for the evaluation of treatment efficacy, adjustment of treatment strategies, and prediction of outcomes for patients with BC and BMs.

## Acknowledgments

*Funding:* This work was supported by the "1+X" Plan of The Second Hospital of Dalian Medical University (Nos. 2022LCJSGC13, 2022LCJSZD03, and 2022MDTZY01), the Wu Jieping Medical Foundation (No. 320.6750.2022-19-18 to C.S.), and the Cultivating Scientific Research Project of The Second Hospital of Dalian Medical University (No. dy2yynpy202215).

 

## Footnote

*Reporting Checklist:* The authors have completed the STROBE reporting checklist. Available at https://qims.amegroups.com/article/view/10.21037/qims-23-1738/rc

*Conflicts of Interest:* All authors have completed the ICMJE uniform disclosure form (available at https://qims.amegroups.com/article/view/10.21037/qims-23-1738/coif). The authors have no conflicts of interest to declare.

*Ethical Statement:* The authors are accountable for all aspects of the work in ensuring that questions related to the accuracy or integrity of any part of the work are appropriately investigated and resolved. This study was conducted in accordance with the Declaration of Helsinki (as revised in 2013) and was approved by the Ethics Committee of The Second Hospital of Dalian Medical University (2022-103). The requirement for individual consent in this retrospective analysis was waived.



## References

1. Sung H, Ferlay J, Siegel RL, Laversanne M, Soerjomataram I, Jemal A, Bray F. Global Cancer Statistics 2020: GLOBOCAN Estimates of Incidence and Mortality Worldwide for 36 Cancers in 185 Countries. CA Cancer J Clin 2021;71:209-49.
2. Siegel RL, Miller KD, Fuchs HE, Jemal A. Cancer statistics, 2022. CA Cancer J Clin 2022;72:7-33.
3. Wang R, Zhu Y, Liu X, Liao X, He J, Niu L. The Clinicopathological features and survival outcomes of patients with different metastatic sites in stage IV breast cancer. BMC Cancer 2019;19:1091.
4. Riggio AI, Varley KE, Welm AL. The lingering mysteries of metastatic recurrence in breast cancer. Br J Cancer 2021;124:13-26.
5. Eisenhauer EA, Therasse P, Bogaerts J, Schwartz LH, Sargent D, Ford R, Dancey J, Arbuck S, Gwyther S, Mooney M, Rubinstein L, Shankar L, Dodd L, Kaplan R, Lacombe D, Verweij J. New response evaluation criteria in solid tumours: revised RECIST guideline (version 1.1). Eur J Cancer 2009;45:228-47.
6. Ban J, Fock V, Aryee DNT, Kovar H. Mechanisms, Diagnosis and Treatment of Bone Metastases. Cells 2021;10:2944.
7. Hayward JL, Carbone PP, Heusen JC, Kumaoka S, Segaloff A, Rubens RD. Assessment of response to therapy in advanced breast cancer. Br J Cancer 1977;35:292-8.
8. Palmer MK. WHO Handbook for Reporting Results of Cancer Treatment. Br J Cancer 1982;45:484-5.
9. Hamaoka T, Madewell JE, Podoloff DA, Hortobagyi GN, Ueno NT. Bone imaging in metastatic breast cancer. J Clin Oncol 2004;22:2942-53.
10. Young H, Baum R, Cremerius U, Herholz K, Hoekstra O, Lammertsma AA, Pruim J, Price P. Measurement of clinical and subclinical tumour response using [18F]-fluorodeoxyglucose and positron emission tomography: review and 1999 EORTC recommendations. European Organization for Research and Treatment of Cancer (EORTC) PET Study Group. Eur J Cancer 1999;35:1773-82.
11. Wahl RL, Jacene H, Kasamon Y, Lodge MA. From RECIST to PERCIST: Evolving Considerations for PET response criteria in solid tumors. J Nucl Med 2009;50 Suppl 1:122S-50S.
12. Sugihara T, Koizumi M, Koyama M, Terauchi T, Gomi N, Ito Y, Hatake K, Sata N. Bone metastases from breast cancer: associations between morphologic CT patterns and glycolytic activity on PET and bone scintigraphy as well as explorative search for influential factors. Ann Nucl Med 2017;31:719-25.
13. Lee JW, Kim SY, Han SW, Lee JE, Lee HJ, Heo NH, Lee SM. [18F]FDG uptake of bone marrow on PET/CT for predicting distant recurrence in breast cancer patients after surgical resection. EJNMMI Res 2020;10:72.
14. Orcajo-Rincon J, Muñoz-Langa J, Sepúlveda-Sánchez JM, Fernández-Pérez GC, Martínez M, Noriega-Álvarez E, Sanz-Viedma S, Vilanova JC, Luna A. Review of imaging techniques for evaluating morphological and functional responses to the treatment of bone metastases in prostate and breast cancer. Clin Transl Oncol 2022;24:1290-310.
15. Du Y, Cullum I, Illidge TM, Ell PJ. Fusion of metabolic function and morphology: sequential [18F] fluorodeoxyglucose positron-emission tomography/computed tomography studies yield new insights into the

 

natural history of bone metastases in breast cancer. J Clin Oncol 2007;25:3440-7.
16. Gherghe M, Mutuleanu MD, Stanciu AE, Irimescu I, Lazar AM, Toma RV, Trifanescu OG, Anghel RM. Quantitative Assessment of Treatment Response in Metastatic Breast Cancer Patients by SPECT-CT Bone Imaging-Getting Closer to PET-CT. Cancers (Basel) 2023;15:696.
17. Li X, An C, Zhang W. Is it sufficient to evaluate metastatic bone involvement in breast cancer using SPECT/CT? A new approach of SPECT/CT-guided targeted bone marrow biopsy. BMC Cancer 2022;22:614.
18. Al-Muqbel KM, Yaghan RJ. Effectiveness of 18F-FDG-PET/CT vs Bone Scintigraphy in Treatment Response Assessment of Bone Metastases in Breast Cancer. Medicine (Baltimore) 2016;95:e3753.
19. Bhoriwal S, Deo SVS, Kumar R, Thulkar S, Gogia A, Sharma DN, Mathur S. A Prospective Study Comparing the Role of 18 FDG PET-CT with Contrast-Enhanced Computed Tomography and Tc99m Bone Scan for Staging Locally Advanced Breast Cancer. Indian J Surg Oncol 2021;12:266-71.
20. Bruckmann NM, Kirchner J, Umutlu L, Fendler WP, Seifert R, Herrmann K, Bittner AK, Hoffmann O, Mohrmann S, Antke C, Schimmöller L, Ingenwerth M, Breuckmann K, Stang A, Buchbender C, Antoch G, Sawicki LM. Prospective comparison of the diagnostic accuracy of 18F-FDG PET/MRI, MRI, CT, and bone scintigraphy for the detection of bone metastases in the initial staging of primary breast cancer patients. Eur Radiol 2021;31:8714-24.
21. Cook GJ, Azad GK, Goh V. Imaging Bone Metastases in Breast Cancer: Staging and Response Assessment. J Nucl Med 2016;57 Suppl 1:27S-33S.
22. Cook GJR, Goh V. Molecular Imaging of Bone Metastases and Their Response to Therapy. J Nucl Med 2020;61:799-806.
23. Cristo Santos J, Henriques Abreu M, Seoane Santos M, Duarte H, Alpoim T, Próspero I, Sousa S, Henriques Abreu P. Bone Metastases Detection in Patients with Breast Cancer: Does Bone Scintigraphy Add Information to PET/CT? Oncologist 2023;28:e600-5.
24. Zamagni C, Gion M, Mariani L, Stieber P, Rubino D, Fanti S, Baum RP, Wirtz RM, Hakim R, Bernardi A, Cacciari N, Quercia S, Fini A, Lenzi M, Pizzirani C, Pagliaro M, Tomasini S, Toracchio S, Carapelle M, Barbieri E. CEA, CA15.3 and 18-FDG PET in the follow-up of early breast cancer (BC) patients (pts): A prospective, multicentric, randomized trial—KRONOS patient-oriented new surveillance study Italy. J Clin Oncol 2007;35:abstr TPS11627.
25. Makhlin I, Korhonen KE, Martin ML, Gillman J, Schubert E, Pantel AR, Mankoff DA, Clark AS. (18)F-FDG PET/CT for the Evaluation of Therapy Response in Hormone Receptor-Positive Bone-Dominant Metastatic Breast Cancer. Radiol Imaging Cancer 2022;4:e220032.
26. Tinterri C, Di Maria Grimaldi S, Sagona A, Barbieri E, Darwish S, Bottini A, Canavese G, Gentile D. Comparison of Long-Term Oncological Results in Young Women with Breast Cancer between BRCA-Mutation Carriers Versus Non-Carriers: How Tumor and Genetic Risk Factors Influence the Clinical Prognosis. Cancers (Basel) 2023;15:4177.
27. Miricescu D, Totan A, Stanescu-Spinu II, Badoiu SC, Stefani C, Greabu M. PI3K/AKT/mTOR Signaling Pathway in Breast Cancer: From Molecular Landscape to Clinical Aspects. Int J Mol Sci 2020;22:173.
28. Urso L, Quartuccio N, Caracciolo M, Evangelista L, Schirone A, Frassoldati A, Arnone G, Panareo S, Bartolomei M. Impact on the long-term prognosis of FDG PET/CT in luminal-A and luminal-B breast cancer. Nucl Med Commun 2022;43:212-9.
29. Suto H, Inui Y, Okamura A. Is CT or FDG-PET more useful for evaluation of the treatment response in metastatic HER2-positive breast cancer? a case report and literature review. Front Oncol 2023;13:1158797.
30. Kitajima K, Fukushima K, Miyoshi Y, Nishimukai A, Hirota S, Igarashi Y, Katsuura T, Maruyama K, Hirota S. Association between $^{18}$F-FDG uptake and molecular subtype of breast cancer. Eur J Nucl Med Mol Imaging 2015;42:1371-7.
31. Boers J, Eisses B, Zwager MC, van Geel JJL, Bensch F, de Vries EFJ, et al. Correlation between Histopathological Prognostic Tumor Characteristics and [18F]FDG Uptake in Corresponding Metastases in Newly Diagnosed Metastatic Breast Cancer. Diagnostics (Basel) 2024;14:416.
32. Kitajima K, Miyoshi Y. Present and future role of FDG-PET/CT imaging in the management of breast cancer. Jpn J Radiol 2016;34:167-80.

**Cite this article as:** Lin R, Lv H, Yu J, Song C, Tian A. 18F-fluorodeoxyglucose positron emission tomography-computed tomography in the localization of the lesions in the osteogenic region of breast cancer bone metastases after therapy. Quant Imaging Med Surg 2024;14(7):4950-4964. doi: 10.21037/qims-23-1738

 